

Density staircases generated by symmetric instability in a cross-equatorial deep western boundary current

F. W. Goldsworth^{1,2}, H. L. Johnson³, D. P. Marshall¹

¹AOPP, Department of Physics, University of Oxford

²Oxford NERC Environmental Research DTP

³Department of Earth Sciences, University of Oxford

Key Points:

- Density staircases are observed in a high-resolution numerical model of a deep western boundary current crossing the equator.
- As the deep western boundary current crosses the equator it becomes symmetrically unstable, generating overturning cells.
- The overturning cells result in differential diapycnal mixing with well mixed regions separated by strongly-stratified mixing barriers.

Corresponding author: Fraser Goldsworth, frasergocean@gmail.com

Abstract

Density staircases are observed in an idealised model of a deep western boundary current upon crossing the equator. We propose that the staircases are generated by the excitement of symmetric instability as the current crosses the equator. The latitude at which symmetric instability is excited can be predicted using simple scaling arguments. Symmetric instability generates overturning cells which, in turn, cause the inhomogeneous mixing of waters with different densities. The mixing barriers and well mixed regions in density profiles coincide, respectively, with the boundaries and centres of the overturning cells generated by the symmetric instability. This new mechanism for producing density staircases may require us to re-evaluate the origins of some of the density staircases observed in the Tropical Atlantic.

Plain Language Summary

In this study we demonstrate that waters of different density are mixed together in a deep western boundary current as it crosses the equator. We show that this is a result of the excitement of small-scale symmetric instabilities. The mixing generates density staircases which can affect the formation of dense waters and diapycnal mixing — processes which are important for maintaining the Atlantic Meridional Overturning Circulation. We use both a high-resolution numerical model and a simple toy-model to explain how the staircases are generated. Historically, many density staircases have been observed in the region we are studying. We suggest that theories of how these staircases are generated may need revising given the findings of this study.

1 Introduction

The Atlantic Meridional Overturning Circulation (AMOC) is a global scale system of currents that is important for transporting heat, salt and other tracers both laterally and vertically, including between hemispheres (Jackson et al., 2015). As such it plays an important role in the response of the climate system to anthropogenic forcing. There are two important cross-equatorial components to the AMOC — the northward flowing, surface intensified North Brazil Current, and the southward flowing deep western boundary current (Bower et al., 2019). At 5°S, the deep western boundary current transports 25.5 ± 8.3 Sv ($1 \text{ Sv} \equiv 10^6 \text{ m}^3 \text{ s}^{-1}$), at a depth between 1,200 m and 3,600 m below the surface, with a width of approximately 100 km and a peak velocity of around 20 cm s^{-1} (Schott et al., 2005). Goldsworth et al. (2021) show that surface cross-equatorial western boundary currents may be susceptible to symmetric instability, but the susceptibility of deep western boundary currents to symmetric instability remains an open question. In this paper we show not only that deep western boundary currents are susceptible to symmetric instability, but that this instability can result in the formation of density staircases.

Density staircases are step like features which can be seen in plots of seawater density against depth, and they are ubiquitous in the global ocean (Stern, 1960; Schmitt et al., 1987; Melling et al., 1984; Tait & Howe, 1968; Johannessen & Lee, 1974; Lambert & Sturges, 1977). The staircases consist of alternating well mixed regions with low stratification and thin interfaces with high stratification. The high stratification interfaces can form “mixing barriers” which inhibit the vertical transport of water properties such as heat and salt, whereas mixing is enhanced in the low stratification regions. Density staircases can affect both diapycnal mixing and water mass transformation rates (Schmitt et al., 2005), which are known to be important in closing the AMOC’s overturning budget (de Lavergne et al., 2022). Many staircases are thought to form as a result of double diffusive convection, but other staircase generation mechanisms have been identified, such as inhomogeneous mixing (Balmforth et al., 1998).

Symmetric instability is a type of submesoscale instability which occurs when the Ertel potential vorticity of a flow has the opposite sign to the planetary vorticity (Stone, 1966; Hoskins, 1974). The potential vorticity is defined as

$$Q = (\mathbf{f} + \nabla \times \mathbf{u}) \cdot \nabla b, \quad (1)$$

where \mathbf{f} is the planetary vorticity vector, \mathbf{u} is the velocity and $b = -g\rho/\rho_0$ is the buoyancy. Potential vorticity with sign opposite to that of the vertical component of planetary vorticity, $\mathbf{k} \cdot \mathbf{f}$, is typically described as “anomalous”. Anomalous potential vorticity can be generated through mechanical or diabatic forcing, or by changing the sign of planetary vorticity. In a deep western boundary current, to leading order, potential vorticity is conserved as the current is separated from the surface and bottom boundary layers in which mechanical and diabatic forcings can act. This means symmetric instability can only be induced via a change in sign of planetary vorticity, as occurs at the equator. Cross-equatorial symmetric instability is unique in this sense — it need not be confined to either the surface boundary layer or sloping bottom boundary layer (Haine & Marshall, 1998; Wenegrat & Thomas, 2020). A host of recent studies have identified regions where cross-equatorial symmetric instability may be excited (Jakoboski et al., 2022; Goldsworth et al., 2021; Forryan et al., 2021; Zhou et al., 2022).

In section 2 we describe our idealized numerical model of a deep western boundary current crossing the equator. In section 3 we demonstrate the formation of density staircases and the excitement of symmetric instability in the model, and propose that the staircases are generated as a result of the onset of symmetric instability. Simple scaling arguments are used to explain the differences between instabilities seen in deep western boundary currents and in surface intensified currents. Finally, in section 4 we summarise our findings and explain the potential implications of these results.

2 Model configuration

Simulations of an idealised deep western boundary current crossing the equator are performed using the MITgcm (Marshall et al., 1997). The domain size is 600 km in the zonal direction, 3,600 km in the meridional and 4,500 m in the vertical. The horizontal grid spacing is 1 km and the vertical grid spacing 10 m. The time-step is 144 s and the model is integrated for a total of 239 days. The model domain is sited on a β -plane, with the equator placed 2,000 km north of the southern boundary. The meridional gradient in the Coriolis parameter is set to $2.3 \times 10^{-11} \text{ s}^{-1} \text{ m}^{-1}$, and the non-traditional Coriolis parameter to $1.5 \times 10^{-4} \text{ s}^{-1}$.

At the surface, a rigid lid boundary condition is employed. The lateral boundary condition is set to be free-slip and the bottom boundary condition to no-slip. The model has sloping bathymetry which can be seen in figure 1b. The model is initialised by setting the meridional velocity and density profiles to those shown in figure 1b, and with a zonal velocity of zero. The density profile is based on a neutral density (or γ^n) climatology aggregated from the area enclosed by the red rectangle in figure 1a. The model is forced by prescribing the meridional velocity, zonal velocity, and the density, at the northern and southern domain boundaries. The same fields used to initialise the model are used as boundary conditions. A sponge region is placed at both the northern and southern edge of the domain. The northern sponge is 100 km thick and the southern sponge 300 km thick. The inverse relaxation time-scale varies from $1 \times 10^{-5} \text{ s}^{-1}$ (corresponding to a time scale of around 1.2 days) at the outer boundaries to 0 at the inner boundaries. The inverse relaxation time-scale has a tanh shape, with a characteristic length-scale of 5 km in the northern sponge and 10 km in the southern sponge.

A linear equation of state, is used, with a reference density of $1022.73 \text{ kg m}^{-3}$ and thermal expansion coefficient of $2 \times 10^{-4} \text{ K}^{-1}$. The linear equation of state avoids the complexities added by non-linear effects. The thermal diffusion coefficient is set to $1 \times$

112 $10^{-5} \text{ m}^2 \text{ s}^{-1}$. A second order-moment Prather advection scheme with a flux limiter is
 113 employed. Salinity is set to be constant and has no impact on the dynamics. Momen-
 114 tum dissipation is provided by a vertical Laplacian viscosity of $4 \times 10^{-4} \text{ m}^2 \text{ s}^{-1}$ and an
 115 adaptive biharmonic Smagorinsky viscosity. Potential vorticity is calculated using the
 116 C-grid algorithm of Morel et al. (2019).

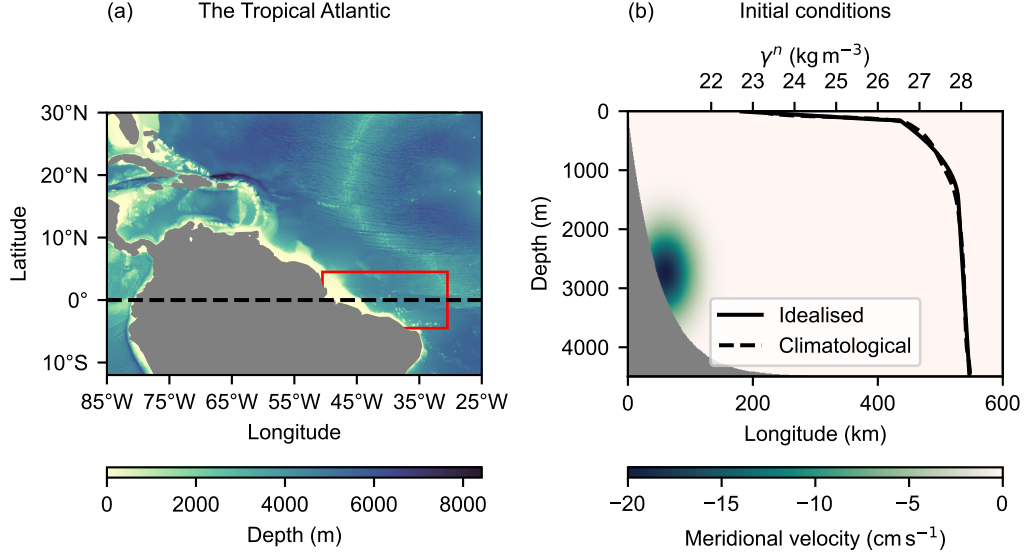


Figure 1. (a) Bathymetric map of the western tropical Atlantic. Climatological profiles of neutral density were aggregated from the area enclosed by the red rectangle. Bathymetry data from GEBCO Compilation Group (2020). (b) Meridional velocity profile (colours) and density profile (solid line) used as initial and boundary conditions for the model. The velocity profile is based on observations by Schott et al. (2005), and the density profile on the climatological mean (dashed line) (Boyer et al., 2018).

3 Symmetric instability and staircase formation

117
 118 Figure 2b shows $\partial_z b$ in the model after 239 days of integration 250 km south of the
 119 equator. Immediately apparent are the thin, sharp regions of high stratification (so called
 120 “mixing barriers”) separating larger regions of well mixed waters with low and uniform
 121 stratification. Moving to 500 km south, we see in figure 2c that some of the weaker bar-
 122 riers have dissipated, however the stronger barriers remain. Figure 2a shows the squared
 123 buoyancy frequency at the equator. At the outer edge of the current’s core we see some
 124 weak mixing barriers.

125 Figure 3a shows the average of the meridional component of relative vorticity be-
 126 tween 234 and 239 days of model integration in a region 250 km south of the equator.
 127 This can be thought of as a crude proxy for a zonal overturning streamfunction — it mea-
 128 sures the local rotation around the meridional axis, i.e. the amount of zonal overturn-
 129 ing. We consider it here as the true zonal overturning streamfunction is ill-defined, since
 130 the flow is not invariant in the meridional direction. Examining the meridional vortic-
 131 ity, note that there are a series of counter-rotating stacked overturning cells between around

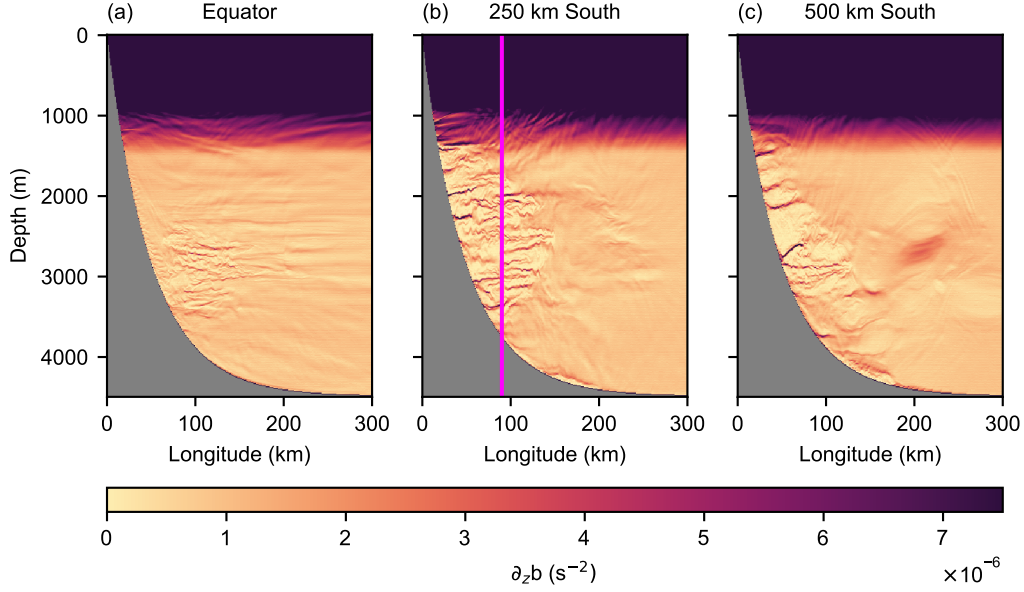


Figure 2. Squared buoyancy frequency after 239 days of model integration plotted at (a) the equator, (b) 250 km south of the equator and (c) 500 km south of the equator. The figures show the presence of mixing barriers (thin filaments of strong stratification) separated by well mixed regions of low stratification. The magenta line indicates the location of the vorticity and density profiles shown in figure 3.

1,750 m and 3,500 m below the surface. The black contours overlain show $\partial_z b = 2 \times 10^{-6} \text{ s}^{-2}$ and help identify the locations of the mixing barriers in figure 2b. We can see that the structure of the buoyancy frequency squared and the meridional vorticity are remarkably similar, with the horizontal edges of the overturning cells (vorticity zeros) approximately coinciding with the locations of the mixing barriers. This is shown more clearly in figure 3b. The black line shows neutral density plotted as a function of depth at 250 km south and 90 km west (the location of the magenta lines and points shown in the other figures). The orange line shows the meridional component of relative vorticity at the same point. Both quantities have been averaged over the time period spanning 234 to 239 days. The treads of the steps in neutral density correspond to mixing barriers and the risers to well mixed regions. When comparing neutral density and the meridional vorticity we again see that the mixing barriers tend to coincide with vorticity zeros, whereas the mixing barriers coincide with vorticity extrema. This suggests that the inhomogeneous mixing driven by the overturning cells is what is causing the formation of the staircases.

3.1 A very simple model of staircase formation

The differential mixing which produces the mixing barriers is analogous to the process which produces zonal jets on a β -plane (Manfroi & Young, 1999). Here, instead of a meridional gradient in planetary vorticity there is a vertical gradient in buoyancy, and instead of mixing in the horizontal plane we have overturning in the vertical plane. We can reproduce the formation of mixing barriers with a toy model, in which we consider how buoyancy changes over time as a result of diffusion and advection by overturning cells. If we express the overturning motion as a streamfunction ψ where $u = -\partial_z \psi$ and

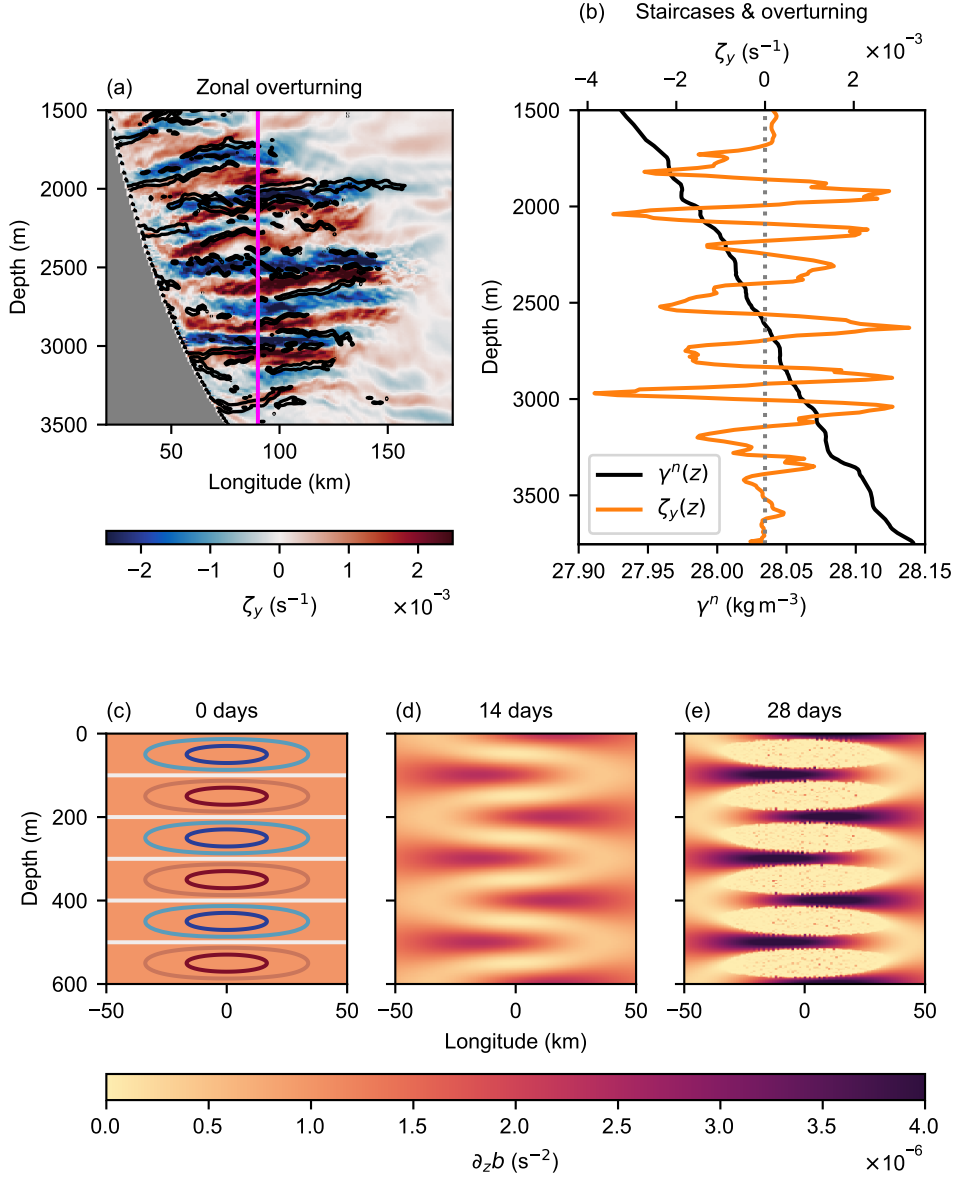


Figure 3. (a) Time mean meridional component of relative vorticity between 234 and 239 days of model integration, plotted as a function of longitude and depth, at 250 km south. Alternating red and blue cells indicate the presence of stacked zonal overturning cells. Overlain is the contour defined by $\partial_z b = 2 \times 10^{-6} \text{ s}^{-2}$, indicating the locations of the mixing barriers. (b) Density (black line) and time mean meridional component of relative vorticity (orange line) plotted as a function of depth at 90 km west and 250 km south (shown on other figures as a magenta line or point). Vorticity extrema coincide with well mixed regions and zeros with mixing barriers suggesting the density staircases are formed by the overturning cells. Panels (c-e) show snapshots of the stratification over time from the toy model, showing how the mixing barriers begin to form in the presence of inhomogeneous mixing. The contours on panel (c) show the overturning stream-function.

$w = \partial_x \psi$ and use a constant harmonic diffusivity, κ we can express the evolution of b as

$$\frac{\partial b}{\partial t} = \frac{\partial \psi}{\partial z} \frac{\partial b}{\partial x} - \frac{\partial \psi}{\partial x} \frac{\partial b}{\partial z} + \kappa \frac{\partial^2 b}{\partial z^2}. \quad (2)$$

We choose $\psi = e^{-x^2/2\sigma^2} \sin(k_z z)$, to represent stacked overturning cells which are localised to a region of width σ in the horizontal. We also set $b(t=0) = N^2 z$, and then solve the equation numerically using a 3rd order Adam's Bashforth scheme on a domain stretching from -50 km to 50 km in the horizontal and spanning 600 m in the vertical. We set $\sigma = 25$ km, $k_z = 2\pi/200 \text{ m}^{-1}$, $\kappa = 1 \times 10^{-5} \text{ m}^2 \text{ s}^{-1}$ and $N^2 = 1 \times 10^{-6} \text{ s}^{-2}$. The grid spacing is set to 1 km in the horizontal and 2.5 m in the vertical, and the time step is 240 seconds. Gravitational instability is parameterised by setting κ to an enhanced value of $5 \times 10^{-3} \text{ m}^2 \text{ s}^{-1}$ in regions where $\partial_z b \leq 0$.

The stratification is shown at three different times in figures 3 (c-e). Alternating high and low stratification regions develop with time. Initially this is a result of differential mixing; however, at later times the mixing barriers become sharper and start to form filaments due to gravitational instability in the low stratification regions producing extra mixing.

3.2 But what is generating the overturning?

Previous work by Goldsworth et al. (2021) has demonstrated that western boundary currents can become unstable when crossing the equator as they advect anomalous potential vorticity from one hemisphere into the other. In figure 4a, which shows the potential vorticity on the $\gamma^n = 28.04$ surface, we can see the advection of positive potential vorticity from the northern hemisphere into the southern hemisphere, so we may expect to see symmetric instability excited south of the equator. The excitement of the instability is apparent in a region from around 25 km to 600 km south of the equator. Figures 4b, c, and d show the potential vorticity as a function of depth and longitude at, the equator, 250 km south and 500 km south respectively, after 239 days of model integration. At the equator we see the advection of waters with anomalous potential vorticity into the southern hemisphere. At 250 km south we can see the excitement of symmetric instability, and by 500 km south we can see large pools of neutral potential vorticity suggesting the waters here have experienced symmetric instability, with the excitement of symmetric instability still underway at around 3,000 m. In figure 4b we also see symmetric instability like patterns in a region of negative potential vorticity. This suggests these waters with negative potential vorticity were undergoing symmetric instability in the northern hemisphere before being advected south of the equator. This also explains the presence of the weak staircases at the equator seen in figure 2a.

3.3 Estimating at which latitudes symmetric instability occurs

Unlike in the study of Goldsworth et al. (2021), we see the excitement of symmetric instability close to the equator followed by the formation of eddies, whereas in the former study we see the spinning up of large anti-cyclonic eddies followed by the excitement of symmetric instability further away from the equator. This is due to the reduced growth rate of barotropic instability in the deep western boundary current, meaning that symmetric instability dominates over short time-scales. This is further exacerbated by the anti-cyclonic eddies seen by Goldsworth et al. (2021), which act to reduce the growth rate of the symmetric instability in their experiments, allowing anomalous potential vorticity to persist whilst the eddies grow (Buckingham et al., 2021).

We can in fact be more quantitative about the latitude at which the instability is forming. There is an e -folding timescale, τ_e , associated with symmetric instability which can be converted into an advective meridional length scale, y with the equation $y = V\tau_e$, where V is a typical meridional velocity. From linear stability theory we know that for

a parallel shear flow, like a deep western boundary current (Hoskins, 1974) the time scale of symmetric instability is given by

$$\tau_e \sim \left(\beta y \left(f + \frac{V}{L_x} \right) \right)^{-1/2} \quad (3)$$

and that for the case of an eddy, such as a North Brazil Current ring, the symmetric instability timescale is (Buckingham et al., 2021)

$$\tau_e \sim \left(\beta y \left(f + \frac{2V}{R} \right) \right)^{-1/2}. \quad (4)$$

We can then convert these expressions to a meridional length scale, giving

$$y \sim \sqrt[3]{\frac{VL_x}{\beta}} \quad (5)$$

for parallel shear flows, and for an eddy

$$y \sim \sqrt[3]{\frac{2VR}{\beta}}. \quad (6)$$

In the case of the eddying flow, we have assumed the meridional velocity is of a similar order of magnitude to the azimuthal velocity. In both expressions we have assumed y to be small and only considered terms of the lowest order in y . We can now evaluate the expressions for the latitude of the onset of symmetric instability. For the deep western boundary current we choose $V \sim 0.2 \text{ m s}^{-1}$, $L_x \sim 30 \text{ km}$ and $\beta \sim 2.3 \times 10^{-11} \text{ m}^{-1} \text{ s}^{-1}$, giving $y \sim 60 \text{ km}$. For the North Brazil Current rings we choose $V \sim 1 \text{ m s}^{-1}$, $R \sim 100 \text{ km}$ and the same value for β , giving $y \sim 200 \text{ km}$. These predictions of the latitude of instability are of the same order of magnitude as those we see in the numerical models. In the case of North Brazil Current rings, Goldsworth et al. (2021) see instability at around 400 km north, and in this study we see instability from around 25 km north of the equator.

4 Conclusions

Density staircases are step like features which become apparent when density is plotted as a function of depth and are common throughout the Earth's oceans. In an idealised model of a deep western boundary current crossing the equator we see density staircases form. The staircases are generated by overturning cells which are in turn generated by the excitement of symmetric instability as the current crosses the equator. Symmetric instability in cross-equatorial flows is excited due to the advection of anomalous potential vorticity from one hemisphere to another. The stacked overturning cells that generate the staircases are, however, a feature of symmetric instability regardless of what is forcing it, suggesting we may see staircase formation in other symmetrically unstable flows, including when anomalous potential vorticity is induced by frictional torques or diabatic processes. Differences in the latitude of instability between surface intensified western boundary currents and deep western boundary currents can be adequately explained using simple scaling arguments relating to growth rates of symmetric instability and advective timescales.

It is thought that diapycnal mixing may play an important role in closing the overturning budget of the Atlantic Meridional Overturning Circulation's deep limb. Figures 2 and 4 clearly show that vigorous mixing is taking place; however, accurately calculating the amount of mixing that is occurring is tricky. This is due to the importance of secondary Kelvin Helmholtz instabilities in transforming water masses. In order to resolve these processes we would need a model with around 40 times the resolution used

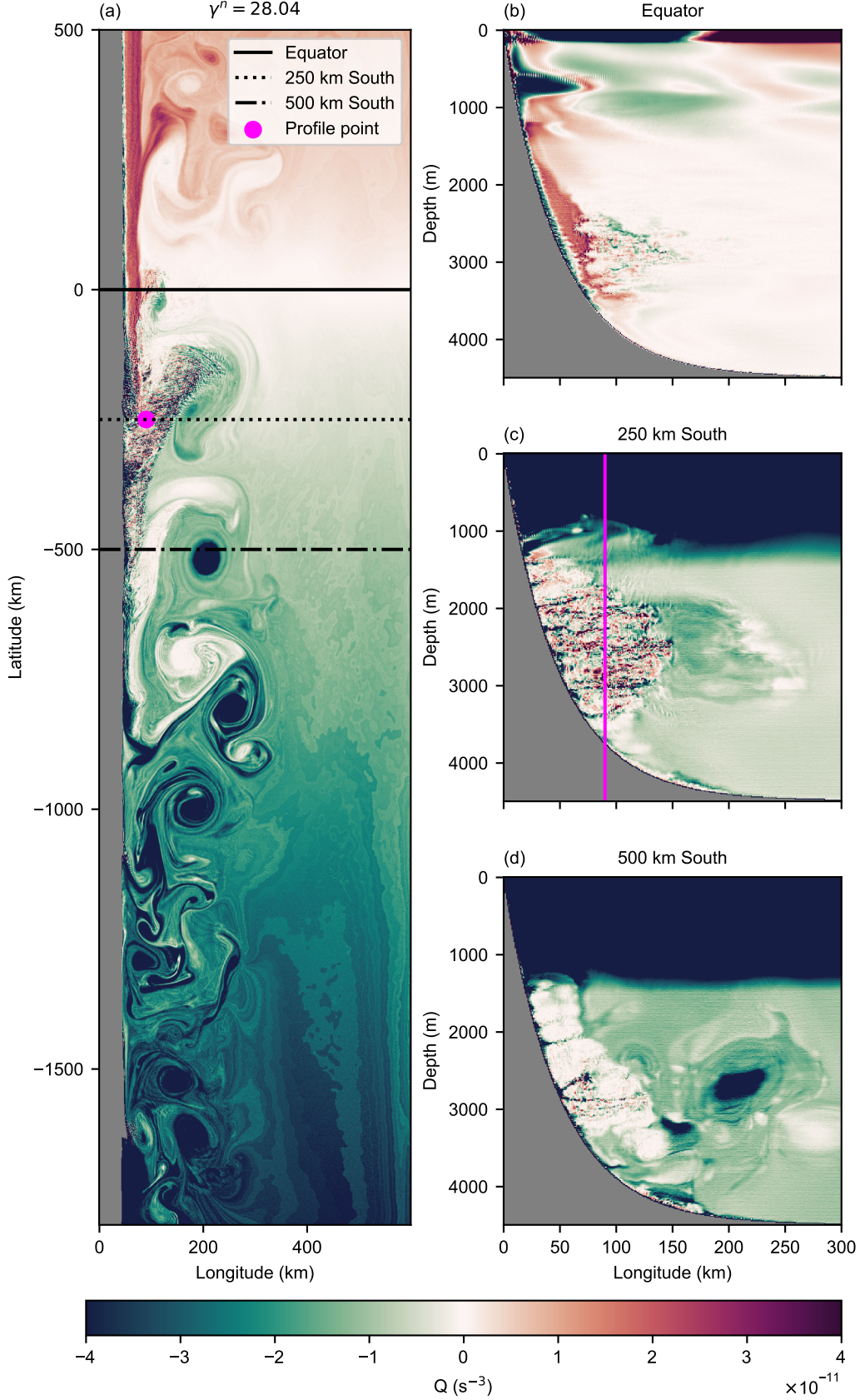


Figure 4. Potential vorticity after 239 days of model integration plotted on (a) the $\gamma^n = 28.04$ surface, (b) at the equator, (c) at 250 km south of the equator, and (d) at 500 km south of the equator. Black lines show the latitudes at which sections have been plotted. The figures show the advection of anomalous potential vorticity from the northern hemisphere into the southern hemisphere and the excitement of symmetric instability. The magenta line and point indicate the location of the vorticity and density profiles shown in figure 3.

here, which is computationally infeasible — such a model would require at least 10^4 times more computational resources to run. Simplified two dimensional models may help in accurately quantifying the induced diapycnal mixing, however.

Density staircases are well documented in the Tropical Atlantic and are often said to form as a result of salt fingering and double diffusive convection (e.g. Schmitt et al. (1987, 2005)). In light of this work, we suggest new insights into mixing in the region could be gained by revisiting existing observations and reexamining the origins of observed staircases.

5 Open Research

Model integrations were run using the MITgcm model (checkpoint 68i) (*MITgcm*, 2019) on the ARCHER2 HPC facility. The git repository Goldsworth et al. (2022b) contains model configuration files, and the python scripts used for analysing the model output. The repository Goldsworth et al. (2022a) contains the data required to recreate the model's initial conditions and a subset of processed model output. The analysis performed on the data made heavy use of the open source xarray (Hoyer & Hamman, 2017) and Dask (Dask Development Team, 2016) software libraries.

Acknowledgments

We are grateful for the financial support of the Natural Environment Research Council NE/L002612/1. This work used the ARCHER2 UK National Supercomputing Service (<https://www.archer2.ac.uk>).

References

- Balmforth, N. J., Llewellyn Smith, S. G., & Young, W. R. (1998, jan). Dynamics of interfaces and layers in a stratified turbulent fluid. *Journal of Fluid Mechanics*, 355, 329–358. Retrieved from <https://www.cambridge.org/core/product/identifier/S0022112097007970/type/journal-article> doi: 10.1017/S0022112097007970
- Bower, A., Lozier, S., Biastoch, A., Drouin, K., Foukal, N., Furey, H., ... Zou, S. (2019). Lagrangian Views of the Pathways of the Atlantic Meridional Overturning Circulation. *Journal of Geophysical Research: Oceans*, 124(8), 5313–5335. doi: 10.1029/2019JC015014
- Boyer, T. P., Garcia, H. E., Locarnini, R. A., Zweng, M. M., Mishonov, A. V., Reagan, J. R., ... Smolyar, I. V. (2018). *World Ocean Atlas 2018. Temperature and salinity*. Retrieved from <https://www.ncei.noaa.gov/archive/accession/NCEI-WOA18> (17/05/2022)
- Buckingham, C. E., Gula, J., & Carton, X. (2021). The role of curvature in modifying frontal instabilities. part i: Review of theory and presentation of a non-dimensional instability criterion. *Journal of Physical Oceanography*, 51(2), 299–315. Retrieved from <https://journals.ametsoc.org/view/journals/phoc/51/2/jpo-d-19-0265.1.xml> doi: 10.1175/JPO-D-19-0265.1
- Dask Development Team. (2016). Dask: Library for dynamic task scheduling [Computer software manual]. Retrieved from <https://dask.org>
- de Lavergne, C., Groeskamp, S., Zika, J., & Johnson, H. L. (2022). Chapter 3 - the role of mixing in the large-scale ocean circulation. In M. Meredith & A. Naveira Garabato (Eds.), *Ocean mixing* (p. 35-63). Elsevier. Retrieved from <https://www.sciencedirect.com/science/article/pii/B9780128215128000104> doi: <https://doi.org/10.1016/B978-0-12-821512-8.00010-4>
- Forryan, A., Naveira Garabato, A. C., Vic, C., Nurser, A. J., & Hearn, A. R.

- (2021). Galápagos upwelling driven by localized wind–front interactions. *Scientific Reports*, 11(1), 1–12. Retrieved from <https://doi.org/10.1038/s41598-020-80609-2> doi: 10.1038/s41598-020-80609-2
- GEBCO Compilation Group. (2020). *Gebco 2020 grid*. doi: 10.5285/a29c5465-b138-234d-e053-6c86abc040b9
- Goldsworth, F. W., Johnson, H. L., & Marshall, D. P. (2022a). *Data for “Density staircases generated by symmetric instability in a cross-equatorial deep western boundary current”*. (dataset) doi: 10.5281/zenodo.6561188
- Goldsworth, F. W., Johnson, H. L., & Marshall, D. P. (2022b). *dwbc-proj*. Retrieved from <https://www.github.com/fraserwg/dwbc-proj> doi: 10.5281/zenodo.7015585
- Goldsworth, F. W., Marshall, D. P., & Johnson, H. L. (2021). Symmetric instability in cross-equatorial western boundary currents. *Journal of Physical Oceanography*, -1(aop), 2049–2067. Retrieved from <https://journals.ametsoc.org/view/journals/phoc/aop/JP0-D-20-0273.1/JP0-D-20-0273.1.xml> doi: 10.1175/JPO-D-20-0273.1
- Haine, T. W. N., & Marshall, J. (1998, apr). Gravitational, Symmetric, and Baroclinic Instability of the Ocean Mixed Layer. *Journal of Physical Oceanography*, 28(4), 634–658. Retrieved from [http://journals.ametsoc.org/doi/abs/10.1175/1520-0485\(1998\)028<0634:gsabio>2.0.co;2](http://journals.ametsoc.org/doi/abs/10.1175/1520-0485(1998)028<0634:gsabio>2.0.co;2) doi: 10.1175/1520-0485(1998)028<0634:gsabio>2.0.co;2
- Hoskins, B. J. (1974, jul). The role of potential vorticity in symmetric stability and instability. *Quarterly Journal of the Royal Meteorological Society*, 100(425), 480–482. Retrieved from <http://doi.wiley.com/10.1002/qj.49710042520> doi: 10.1002/qj.49710042520
- Hoyer, S., & Hamman, J. (2017). xarray: N-D labeled arrays and datasets in Python. *Journal of Open Research Software*, 5(1). Retrieved from <https://doi.org/10.5334/jors.148> doi: 10.5334/jors.148
- Jackson, L. C., Kahana, R., Graham, T., Ringer, M. A., Woollings, T., Mecking, J. V., & Wood, R. A. (2015). Global and European climate impacts of a slow-down of the AMOC in a high resolution GCM. *Climate Dynamics*, 45(11-12), 3299–3316. Retrieved from <http://dx.doi.org/10.1007/s00382-015-2540-2> doi: 10.1007/s00382-015-2540-2
- Jakoboski, J., Todd, R. E., Owens, W. B., Karnauskas, K. B., & Rudnick, D. L. (2022, May). Potential Vorticity and Instability in the Pacific Equatorial Undercurrent West of the Galápagos Archipelago. *Journal of Physical Oceanography*. Retrieved 2022-08-04, from <https://journals.ametsoc.org/view/journals/phoc/aop/JP0-D-21-0124.1/JP0-D-21-0124.1.xml> doi: 10.1175/JPO-D-21-0124.1
- Johannessen, O. M., & Lee, O. S. (1974). A deep stepped thermo-haline structure in the Mediterranean. *Deep-Sea Research and Oceanographic Abstracts*, 21(8), 629–639. doi: 10.1016/0011-7471(74)90047-3
- Lambert, R. B., & Sturges, W. (1977, mar). A thermohaline staircase and vertical mixing in the thermocline. *Deep Sea Research*, 24(3), 211–222. Retrieved from <https://linkinghub.elsevier.com/retrieve/pii/S0146629177800015> doi: 10.1016/S0146-6291(77)80001-5
- Manfroi, A. J., & Young, W. R. (1999). Slow evolution of zonal jets on the beta plane. *Journal of the Atmospheric Sciences*, 56(5), 784–800. doi: 10.1175/1520-0469(1999)056<0784:SEOZJO>2.0.CO;2
- Marshall, J., Adcroft, A., Hill, C., Perelman, L., & Heisey, C. (1997). A finite-volume, incompressible navier stokes model for, studies of the ocean on parallel computers. *Journal of Geophysical Research C: Oceans*, 102(C3), 5753–5766. doi: 10.1029/96JC02775
- Melling, H., Lake, R., Topham, D., & Fissel, D. (1984, jan). Oceanic thermal structure in the western Canadian Arctic. *Continental Shelf Research*, 3(3),

- 233–258. Retrieved from [https://linkinghub.elsevier.com/retrieve/pii/](https://linkinghub.elsevier.com/retrieve/pii/S0278434384900104)
0278434384900104 doi: 10.1016/0278-4343(84)90010-4
- MITgcm. (2019). Retrieved from <http://mitgcm.org/>
- Morel, Y., Gula, J., & Ponte, A. (2019). Potential vorticity diagnostics based on
balances between volume integral and boundary conditions. *Ocean Modelling*,
138(April), 23–35. Retrieved from [https://doi.org/10.1016/j.ocemod.2019](https://doi.org/10.1016/j.ocemod.2019.04.004)
.04.004 doi: 10.1016/j.ocemod.2019.04.004
- Schmitt, R. W., Ledwell, J. R., Montgomery, E. T., Polzin, K. L., & Toole, J. M.
(2005). Ocean science: Enhanced diapycnal mixing by salt fingers in the
thermocline of the tropical atlantic. *Science*, 308(5722), 685–688. doi:
10.1126/science.1108678
- Schmitt, R. W., Perkins, H., Boyd, J. D., & Stalcup, M. C. (1987). C-SALT: An
investigation of the thermohaline staircase in the western tropical North At-
lantic. *Deep Sea Research Part A, Oceanographic Research Papers*, 34(10),
1655–1665. doi: 10.1016/0198-0149(87)90014-8
- Schott, F. A., Dengler, M., Zantopp, R., Stramma, L., Fischer, J., & Brandt, P.
(2005). The shallow and deep western boundary circulation of the South At-
lantic at 5°–11°S. *Journal of Physical Oceanography*, 35(11), 2031–2053. doi:
10.1175/JPO2813.1
- Stern, M. E. (1960). The “Salt-Fountain” and Thermohaline Convection. *Tellus*,
12(2), 172–175. doi: 10.3402/tellusa.v12i2.9378
- Stone, P. H. (1966, jul). On Non-Geostrophic Baroclinic Stability. *Journal of the*
Atmospheric Sciences, 23(4), 390–400. Retrieved from [http://journals](http://journals.ametsoc.org/doi/10.1175/1520-0469(1966)023%3C0390:ONGBS%3E2.O.CO;2)
.ametsoc.org/doi/10.1175/1520-0469(1966)023%3C0390:ONGBS%3E2
.O.CO;2 doi: 10.1175/1520-0469(1966)023%3C0390:ONGBS%3E2.O.CO;2
- Tait, R., & Howe, M. (1968, jun). Some observations of thermo-haline stratification
in the deep ocean. *Deep Sea Research and Oceanographic Abstracts*, 15(3),
275–280. Retrieved from [https://linkinghub.elsevier.com/retrieve/pii/](https://linkinghub.elsevier.com/retrieve/pii/S0011747168900053)
0011747168900053 doi: 10.1016/0011-7471(68)90005-3
- Wenegrat, J. O., & Thomas, L. N. (2020). Centrifugal and symmetric instability
during Ekman adjustment of the bottom boundary layer. *Journal of Physical*
Oceanography, 50(6), 1793–1812. doi: 10.1175/JPO-D-20-0027.1
- Zhou, H., Dewar, W., Yang, W., Liu, H., Chen, X., Li, R., ... Gopalakrishnan,
G. (2022). Observations and modeling of symmetric instability in the ocean
interior in the Northwestern Equatorial Pacific. *Communications Earth &*
Environment, 3(1). doi: 10.1038/s43247-022-00362-4